Effects of anatomical constraints on tumor growth

B. Capogrosso Sansone,[1] P. P. Delsanto,[1] M. Magnano,[2,3] and M. Scalerandi[1]
[1]*INFM, Diptimento di Fisica, Politecnico di Torino, Torino, Italy*
[2]*Divisione di Otorinolaringoiatria, Ospedale Mauriziano Umberto I, Torino, Italy*
[3]*Institute for Research and Cancer Care Therapy, Candiolo, Torino, Italy*
(Received 25 July 2000; revised manuscript received 1 December 2000; published 18 July 2001)

Competition for available nutrients and the presence of anatomical barriers are major determinants of tumor growth *in vivo*. We extend a model recently proposed to simulate the growth of neoplasms in real tissues to include geometrical constraints mimicking pressure effects on the tumor surface induced by the presence of rigid or semirigid structures. Different tissues have different diffusivities for nutrients and cells. Despite the simplicity of the approach, based on a few inherently local mechanisms, the numerical results agree qualitatively with clinical data (computed tomography scans of neoplasms) for the larynx and the oral cavity.

DOI: 10.1103/PhysRevE.64.021903 PACS number(s): 87.10.+e, 05.45.−a, 02.70.−c

I. INTRODUCTION

The term ''cancer'' refers to over a hundred different pathologies, each with specific characteristics. Nevertheless, the basic processes that determine the development of a neoplasm are very similar. As a consequence, we can describe the evolution of pathologies in terms of a set of simplified rules, which mimic the local biophysical and biochemical reactions underlying the cellular functions. Several recent models organize the many pieces of biological information available at the cellular level to provide simple but reliable descriptions of the global behavior of tumor cells, such as their dynamics [1] and differentiation [2].

Numerous growth models [3–5] analyze the evolution of clusters of cells, such as tumors, and their interactions with their surrounding environment [6–8]. However, even though the basic processes are generally well understood, the task of predicting the evolution of a single tumor ''*in vivo*'' is beyond current numerical tools. A large number of factors, hard to control, strongly influence tumor growth, e.g., the general condition of the patient, local nutrient availability, anatomy of the location where the tumor develops, malignancy of the tumor cells, etc. Even in *in vitro* experiments, which are much easier to control, specifying accurately the initial and boundary conditions is difficult since stochastic effects are always present.

Nevertheless, mathematical models that aim to describe the physical interactions, both at the intracellular and extracellular level, may help to predict the statistical properties of neoplasms and to optimize therapies. For these purposes, numerical simulations are the tool of choice, since they can include local mechanisms, which are never negligible in biological systems as complex as tumors.

A basic model must include only those processes that determine the growth of neoplasms. The evolution of tumors depends on both cell properties and the environment. Cells behave like particles with an internal energy store, as in a recent model for bacteria [9]. Cells absorb energy from their surroundings (in the form of bound energy of absorbed molecules) and release it in different forms (by disaggregation of chemical bonds). As a consequence of energy conservation, internal energy may be stored and used to build proteins for duplication and/or for damage recovery. We model cell diffusion, absorption and consumption as physical processes in which the stored energy determines the behavior of the cells (e.g., mitosis occurs only if the stored energy is sufficiently large) [10,11]. The availability of energy controls the transitions of cells from one state to another and, as a consequence, limits tumor growth. E.g., suppressing local vascularization (angiogenesis) slows tumor growth [12,13]. Finally, tumor morphology is strongly related to the nutrient gradient [14].

Also, the pressure of the surrounding environment affects strongly the tumor evolution, inhibiting its diffusion and proliferation [15]. On one side elastic effects compress both the healthy tissue and the tumor mass [16,17] and possibly restrict growth. On the other hand, the toughness of the surrounding tissue strongly affects cellular invasion through the action of dygestive enzymes [18].

In previous papers we presented a model, based on the local interaction simulation approach (LISA) [19], which describes the evolution of tumor cells interacting with their environment [6] and the influence on the vascular system of local modifications in cell metabolism [20]. The model neglects explicitly the influence of compression on the tumor evolution. As such it could describe the behavior of neoplasms in soft tissues [21], i.e., tissues without anatomical constraints (such as cartilage, bones, tendons, etc.). Starting from a given set of phenomenological rules, it allowed us to reproduce several commonly observed clinical features such as growth morphologies dependent on the nutrient gradient, formation of a necrotic core, transition from initial slow growth to a catastrophic event, etc. [6]. We also showed that all the possible outcomes of a neoplasm (regression, latency, metastasis, and unlimited growth) may be obtained by varying the ratio between nutrient affinity (a parameter of the cell) and nutrient availability (an environmental parameter) [22].

In the present contribution we extend our model to include the influence of anatomical constraints, which affect both the speed and morphology of tumor development. Bones, tendons, cartilages, etc. have been shown to limit tumor growth, since they limit the available volume and, as a consequence, increase the pressure on the tumor surface. A neoplasm born close to rigid or semirigid tissues finds itself in a particularly hostile environment. As a consequence, tu-

mor growth may be slow, particularly if neoplastic cells are not too aggressive. The tumor remains very localized in the initial stages and latency may often be the outcome if the tumor is not well vascularized. Also, metastasis is likely, since the tumor finds in the vascular tree the easiest way out of its rigid boundaries. Cell adhesion and invasive properties are also influenced by the pressure applied by the surrounding tissue [23]. Only in a few cases does the tumor mass reach a critical threshold and exert a pressure large enough to destroy the tissues of the anatomical barrier.

Section II describes the proposed model, where we predict the evolution of neoplasms in two specific clinical cases (larynx and jaw). We compare the results of the numerical simulations with clinical data [computed tomography (CT) scans].

II. MODEL

We consider a rectangular slab of tissue of size $L \times L'$ and discretize it as a two-dimensional (2D) grid with $N_x \times N_y$ grid elements of sides ε_x and ε_y, respectively We also consider a third dimension z to represent the growth of neoplastic cells, adopting the usual $2+1$ dimension growth representation [24]. This description is quite reasonable for *in vitro* experiments, but is also acceptable in many *in vivo* situations, if the tumor develops in a fold between two epithelial surfaces without infiltration into the healthy tissue. Several anatomical regions have a quasi-2D conformation, either due to translational symmetry along the z direction or because of anatomical constraints that inhibit growth in one direction, normal to the plane (such as tumors affecting the tongue or the jaw).

Each cell of the grid is represented by a grid node (i,j) located in its center. At any time and in each node we define a total lateral surface of capillaries S_{ij}^t, a number of molecules of nutrient p_{ij}^t, and a number of cells, belonging to different populations: healthy cells h_{ij}^t, cancer cells c_{ij}^t, and necrotic cells d_{ij}^t. S_{ij}^t represents the source of energy and its spatial inhomogeneity allows us to describe regions of the tissue with different vascularization.

The tumor pressure may affect the spatial distribution of capillaries. For simplicity we consider a single nutrient, representing a mixture of all nutrients necessary for cells survival. Nutrient molecules diffuse through the vessel walls into the tissue except in the regions occupied by bone or cartilage, which are not vascularized $(S_{ij}^t=0)$. We assume that healthy cells have no specific metabolism, but rather that they behave as a sink for nutrients, since they absorb it at a constant rate. Cancer cells have a complex metabolism as described in Sec. II A. Finally, necrotic cells are completely inactive and are slowly reabsorbed by the tissue due to the action of specific antibodies (macrophages).

The spatiotemporal evolution of the tumor obeys a set of iteration equations that keep into account three different factors, as described in Secs. II A, II B, and II C, which are related to (i) properties of the cells and their state transitions, (ii) pressure due to the presence of anatomical constraints, and (iii) limited energy availability.

A. Neoplastic cell metabolism

We consider here only two basic cellular activities: absorption of nutrients and their consumption. At each time step, neoplastic cells absorb a certain amount of nutrient γ_{ij}^t and transform it into intracellular energy σ_{ij}^t through ''transporters'' expressed on the cell membrane. Cancer cells have a much larger affinity for nutrients than healthy ones. The number of transporters per cell, Γ, defines the tumor aggressiveness, which is also affected by the environmental conditions. Each active transporter absorbs a fixed amount of nutrient δ, but the number of active transporters depends on the local nutrient concentration. Since time is also discrete, we can write the amount of nutrient absorbed by each cell at the site (i,j) in the time interval $(t,t+1)$ as

$$\gamma_{ij}^t = \Gamma\,\delta\left[1-\exp\left(-\frac{p_{ij}^t}{\Gamma\,\delta\cdot c_{ij}^t}\right)\right], \tag{1}$$

where $\Gamma\,\delta$ represents the maximum amount of absorbed nutrient (i.e. when all the transporters are active), c_{ij}^t is the number of cells located at the current node and we assume an exponential saturation in order to account for the partial inactivation of transporters when the amount of available nutrient p_{ij}^t is low.

The absorbed nutrient is partly consumed to perform the metabolic functions that keep the cell alive: we call β the amount of consumed nutrient per neoplastic cell. The remainder is stored as an energy reserve inside the cell. As a consequence of the absorption and consumption, three situations may take place depending on the amount of previously stored energy σ_{ij}^t.

(1) If $\sigma_{ij}^t+\gamma_{ij}^t-\beta<0$ cellular death (apoptosis) occurs,

$$c_{ij}^{t+1}=(1-\lambda_{ij}^t)c_{ij}^t,$$

$$d_{ij}^{t+1}=d_{ij}^t+\lambda_{ij}^t c_{ij}^t, \tag{2}$$

where λ_{ij}^t represents the apoptosis rate. A choice such as

$$\lambda_{ij}^t=1-\frac{\sigma_{ij}^t+\gamma_{ij}^t}{\beta}$$

insures that the absorbed nutrient is equal to the amount consumed by all the cells that have survived the apoptotic event. As a consequence

$$\sigma_{ij}^{t+1}=0.$$

(2) If $0\leqslant\sigma_{ij}^t+\gamma_{ij}^t-\beta\leqslant Q_m$ cells are in a normal metabolic state (Q_m is the threshold for mitosis), i.e., neither duplication nor death occur. The excess energy is stored as internal energy σ_{ij}^t,

$$c_{ij}^{t+1}=c_{ij}^t,$$

$$d_{ij}^{t+1}=d_{ij}^t, \tag{3}$$

$$\sigma_{ij}^{t+1}=\sigma_{ij}^t+\gamma_{ij}^t-\beta.$$

(3) If $\sigma_{ij}^t+\gamma_{ij}^t-\beta>Q_m$ cellular duplication and subsequent stored energy redistribution occur,

$$c_{ij}^{t+1}=(1+\mu)c_{ij}^t,$$
$$d_{ij}^{t+1}=d_{ij}^t, \tag{4}$$
$$\sigma_{ij}^{t+1}=\frac{\sigma_{ij}^t(1-\eta)}{(1+\mu)},$$

where μ and η are the duplication rate and relative amounts of energy consumed in the duplication, respectively. Low values of the mitosis threshold Q_m correspond to a fast cell cycle time and consequently to a strong tumor malignancy.

B. Environmental pressure

This description of the cellular metabolism does not account for the migration of cells from one node to its neighbors, which is strongly affected by the pressure of the local environment. Neoplastic cells living in a hostile environment (i.e., with insufficient nutrient availability) may detach from the extracellular matrix and diffuse into surrounding tissue. The process is mediated by a digestive enzyme produced by cancer cells, which digest some of the healthy cells surrounding the tumor. Cells detached from the matrix have a short lifetime but a large mobility, which allows them, at least in soft tissues, to diffuse towards regions favorable to proliferation. Often such a process leads to metastasis, i.e., to the migration of cells to a vessel and from there to other body locations. Migration into vessels or into the lymphatic system is highly favored when the tumor is compressed by anatomical constraints, which inhibit its normal expansion in volume [25].

We describe migration by means of a classical diffusion equation, assuming that the diffusion coefficient is zero whenever the available nutrient per cell is larger than a given threshold P_d,

$$c_{ij}^{t+1}=c_{ij}^t+\sum_{i'j'}^{NN}(\tilde{\alpha}_{i'j'}^{ij}c_{i'j'}^t-\tilde{\alpha}_{ij}^{i'j'}c_{ij}^t), \tag{5}$$

where NN denotes all the nearest neighbors and

$$\tilde{\alpha}_{ij}^{i'j'}=\hat{\alpha}_{i'j'}\Theta\left(P_d-\frac{p_{ij}^t}{c_{ij}^t}\right) \tag{6}$$

is the diffusion coefficient from node (ij) to node $(i'j')$ and $\hat{\alpha}_{i'j'}$ is a coefficient that depends only on the properties of the tissue at the node $i'j'$.

In tumors with a large proliferation rate cell division prevails over diffusion. However, cells also diffuse when they duplicate since a large amount of cell division leads to a swift reduction in the amount of nutrient locally available per cell. As a consequence, diffusion coupled to proliferation is an important ingredient in the growth process, since it leads to an increase in tumor size.

The parameter $\hat{\alpha}_{ij}$ allows us to characterize different kinds of tissues. Different tissues have different consistencies and, therefore, different permeabilities to diffusion. In general, hard tissues (such as cartilage and bones) are almost impenetrable ($\hat{\alpha}_{ij}$ almost negligible), while $\hat{\alpha}_{ij}$ is rather large for connective tissue or muscle. When tumor cells reach a given grid node, the consistency of the corresponding tissue changes to a value typical of neoplastic tissues. As a consequence, the final distribution of $\hat{\alpha}_{ij}$ maps the tumor distribution. A tumor mass may often be perceived by touching it and evaluating its consistency empirically.

C. Nutrient sources and diffusion

Nutrient molecules diffuse into the tissue from capillaries that act as sources. The pressure applied by the surrounding tissue affect nutrient diffusion and therefore considerations analogous to the ones presented in Sec. II B apply. We must include the absorption of energy ζ_{ij}^t due to the presence of healthy cells. For the sake of simplicity, we assume this quantity to be uniform and constant: $\zeta_{ij}^t=\zeta_0$. The consumption may vary from node to node according to the kind of tissue.

The spatiotemporal evolution of nutrients obeys the following reaction-diffusion equation:

$$p_{ij}^{t+1}=p_{ij}^t+\sum_{i'j'}^{NN}(\alpha_{ij}p_{i'j'}^t-\alpha_{i'j'}p_{ij}^t)-\gamma_{ij}^t c_{ij}^t-\zeta_{ij}^t+\Psi_{ij}^t, \tag{7}$$

where α_{ij} is the diffusion coefficient for the nutrient. The source term Ψ_{ij}^t tries to restore the equilibrium between the concentrations outside and inside the vessel. However, the flux through the capillary walls has an upper limit proportional to their lateral surface area S_{ij}^t. As a consequence, equilibrium cannot be reached if the nutrient absorption is too large. In the case of nonvascularized tissues, Ψ_{ij}^t is zero. Tissues with a large diffusion coefficient $\hat{\alpha}_{ij}$ for neoplastic cells usually have a large value of α_{ij} whereas α_{ij} almost vanishes in poorly vascularized tissues.

The pressure induced by the tumor mass affects the vascularization. In particular, since the local number of cells (tumor and necrotic) increases, vasoconstriction occurs, i.e., the lateral capillaries surface decreases,

$$S_{ij}^t=S_{ij}^0\exp\left[-\left(\frac{c_{ij}^t+d_{ij}^t}{\Omega}\right)\right], \tag{8}$$

where Ω is a normalization coefficient. This effect helps the formation of a large necrotic core since when $c_{ij}^t+d_{ij}^t\gg\Omega$, capillaries almost completely shut off with consequent local starvation of the cells. We do not consider other mechanisms that can limit blood flow without involving pressure effects.

III. RESULTS AND DISCUSSION

In this section we study the behavior of tumors growing at two different sites of the human neck and head, i.e., in the larynx and oral cavity. Due to their particular anatomy, the proposed $(2+1)$-dimensional approximation applies, particularly for neoplasms located close to the vocal cords (lar-

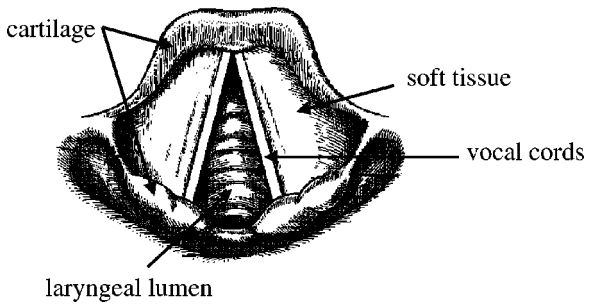

FIG. 1. Schematic representation of larynx anatomy.

ynx) or to the jaw. The spectrum of possible outcomes for these pathologies is quite rich, efficiently testing the capability of the model to predict the evolution of tumors with different intrinsic malignancies. In order to demonstrate the validity of the approach, we first compare the numerical results with CT scans. Then, we briefly discuss some predictions based on the numerical results, which seem to agree, at least qualitatively, with clinical data.

A. Neoplasms of the larynx close to the glottic plane

The larynx forms a cylinder ending in the trachea. Its threefold functions are passage of air, sound emission through vocal cord vibrations, and protection of the tracheobronchial tree by a sphyncter in the glottic plane (upon which the vocal cords lie). It consists (see Fig. 1) of several tissues of different texture separed by a cartilage, which behaves as a barrier, impenetrable to tumor cells, and exerts a pressure that inhibits the growth of the lesion. The vocal cords are intermediate in hardness and separate the soft tissue from the laryngeal lumen, which decreases in diameter when a neoplasm grows on the vocal cords. The vocal cords are set into motion by a tendon that crosses the thyroidal cartilage.

Malignant neoplasms in the larynx are usually strongly aggressive and remarkable in evolution pattern. Since the cartilage splits into two folds in the glottic plane, the latter constitutes a particularly vulnerable area to the formation and progression of a neoplasm even though, in the first stages, the ligament structure may inhibit diffusive growth [26,27]

Table I shows the diffusion coefficients for both cancer cells and nutrients and the total (at $t=0$) capillary lateral surface areas (normalized to the corresponding values for soft tissue) used in the simulations. These ratios agree with the known texture and elastic properties of the tissues. Since neoplastic cells produce digestive enzymes that degrade the surrounding tissue, the coefficient for tumor diffusion into cartilage is nonzero. The capillary lateral surface area agrees with measured capillary concentrations. The values $\hat{\alpha}_s = 0.009$, $\alpha_s = 0.25$, and $S_s^0 = 0.15$ are arbitrary units that have been used in the simulations leading to a satisfactory fitting with CT scans, as shown later.

TABLE I. Diffusion coefficients for cancer cells ($\hat{\alpha}$) and nutrients (α) and capillary distribution for various tissues.

	$\hat{\alpha}/\hat{\alpha}_s$	α/α_s	S^0/S_s^0
Soft tissue	1	1	1
Vocal cords	0.1	0.1	0.9
Tendon region	0.8	0.8	1.2
Cartilage	0.02	0	0
Tumor	0.6	1	

In vivo data suggest that the intrinsic tumor malignancy and local vascular efficiency determine the long term evolution of the neoplasm. In fact, while the original seed of tumor cells is almost always localized in the soft tissue just beneath the vocal cords and grows only in a region between the soft tissue and the vocal cords, four possible outcomes are found in clinical cases.

(1) Nonmalignant tumors usually grow to a small mass and then stop growing. These tumors are seldom observed in clinical practice since they are asymptomatic (latent phase).

(2) A slowly growing nonaggressive tumor develops in the soft connective tissue without affecting the vocal cords (noninvasive phase).

(3) A tumor with intermediate aggressivity attacks the vocal cords and expands into the lumen without gnawing into the cartilage (invasive phase).

(4) An aggressive tumor is characterized by very rapid growth and violent proliferation concomitant with the rupture of the thyroid cartilage (breaking phase).

In the latter two cases the tissues swell in the direction of the free margin of the vocal cord. As shown later, our numerical treatement reproduces all these possible outcomes.

In order to validate our approach, Fig. 2 compares CT scans to the results of our simulations for two tumors with different intrinsic malignancy. In the CT scans (upper plots) dotted lines delimit the tumor masses. The first column displays the behavior of a less aggressive tumor lying on the thyroid cartilage (white in the CT scan and black in the simulation). The numerical results (second row) agree qualitatively with the CT scan maps, both in shape and in size. In particular, a reduced swelling of the tissue towards the lumen (A) and a nesting of the tumor in proximity of the gloctic plane (B) are observed. Also, the tumor gnaws very slowly at the vocal cord, which is not eroded, where the tumor separates from the lumen (C). Also, typical of nonaggressive neoplasms is the horse-shoe shape (noticeable in both the CT scan and simulation results), which surrounds the upper edge of the lumen (D).

A more aggressive tumor (second column of Fig. 2), almost completely occludes the lumen (A), more apparent in the CT scan, due to a relaxation of the vocal cords during the clinical test. The tumor is no longer confined to the larynx, but after partial breaking of the thyroid cartilage, it starts to infiltrate the region just beneath the throat skin (B). Also, the growth is more uniform and the erosion of the vocal cords is fast (C).

In order to emphasize the effects of anatomical constraints, we simulated tumors growing in a tissue with a laryngeal lumen, but with no cartilage or vocal cords. The bottom row of Fig. 2 corresponds to the same time and aggressivity of tumors considered above. In these cases, cells

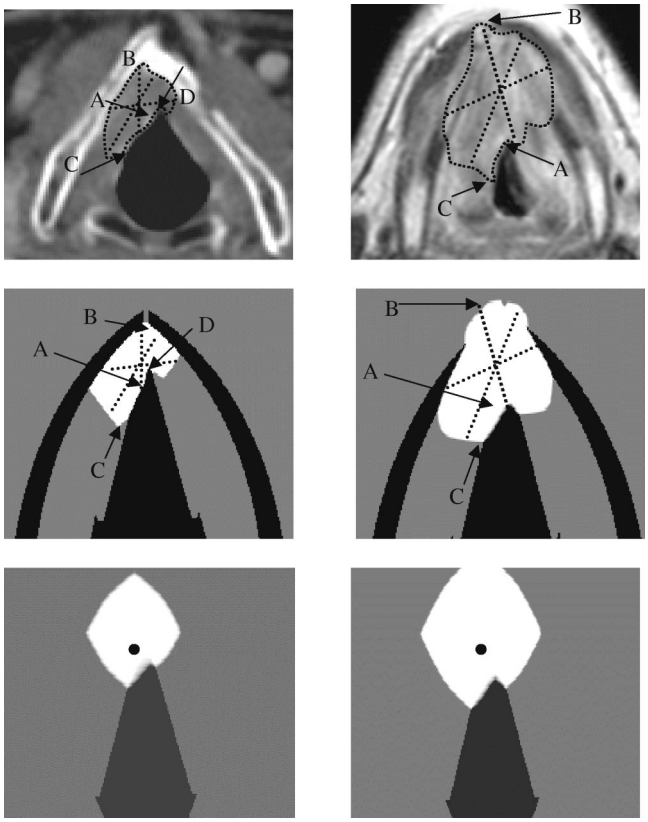

FIG. 2. Comparison between CT scans (first row) and LISA simulations (second row) for two tumors with different malignancy. The bottom row plots refer to tumors growing in a tissue without anatomical constraints. For all simulations, the tumor seed was initially located in the position of the black point shown in the bottom row. Snapshots are at time $T=8000$ and $T=5000$ (arbitrary units) for the left and right columns, respectively.

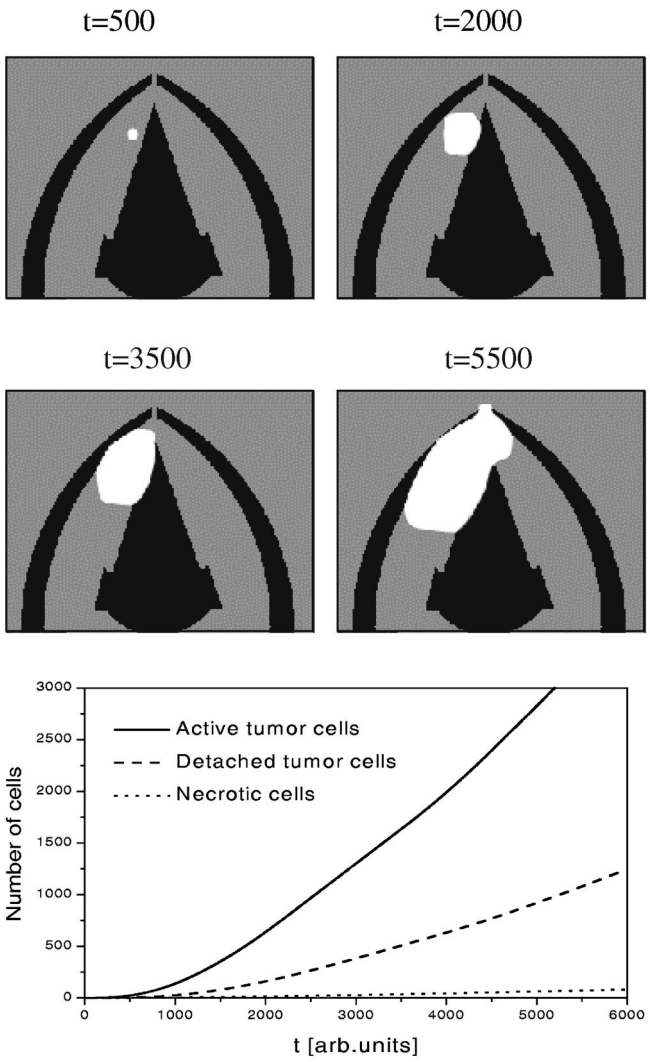

FIG. 3. Snapshots at successive times of the evolution of a very aggressive tumor ($\Gamma=0.03$) in the larynx. Lighter gray tones denote higher densities of neoplastic cells. The cartilage and oral cavity are depicted in black. Times are in arbitrary units. In the bottom, the linear plots represent the time evolution of the number of active, diffusing, and necrotic cells.

division prevails over diffusion since anatomical barriers no longer constrain the blood supply. As a consequence, the tumors grow faster to considerably larger volumes. Tumors are almost spherical and uniformly occlude the upper part of the lumen.

Our approach predicts the time evolution of a neoplasm for different parameter values. Figures 3 and 4 display a sequence of snapshots, which illustrate the behavior of the tumor for two different nutrient affinities Γ, keeping all other parameters fixed. In the first case (Fig. 3, $\Gamma=0.03$), the number of transporters is large and the tumor is very aggressive. The neoplasm initially assumes an almost spherical shape. Nutrient availability has no significant gradient and the anatomical constraints are still far away, so that pressure effects are negligible. At later times ($t\approx2000$) the tumor starts eroding the left vocal cord, causing a local swelling in agreement with clinical observations. Soon after, it also erodes part of the thyroidal cartilage ($t=3500$). However, thyroid deterioration is slow and the tumor mass remains confined inside the larynx until $t\approx5500$. At later times the tumor opens a path through the cartilage plates and violently invades the external soft tissue.

The pressure exerted by anatomical constraints primarily determines the final shape assumed by the neoplasm. However, the formation of a nutrient gradient also plays a significant role. The large consumption by neoplastic cells rapidly leads to a local nutrient depletion and the pressure applied by the growing mass chokes vessels close to the tumor surface (or inside the tumor mass). As a consequence, the growth in the direction parallel to the left vocal cord is quite slow.

In the linear plots, at the bottom of Fig. 3, we observe a swift growth of the tumor to a very large mass with a relatively small necrotic core (due to the good initial vascularization and subsequent action of macrophages). Note also the large number of diffusing cells, which erode the hard tissues. The large volume reached by the tumor accompanies a large increase of density in the region, in agreement with the clinically observed toughening of the tissue.

In Fig. 4, we analyze the temporal evolution for a far less aggressive tumor ($\Gamma=0.003$). Note that the tumor mass is considerably smaller than in the previous case (the grayness

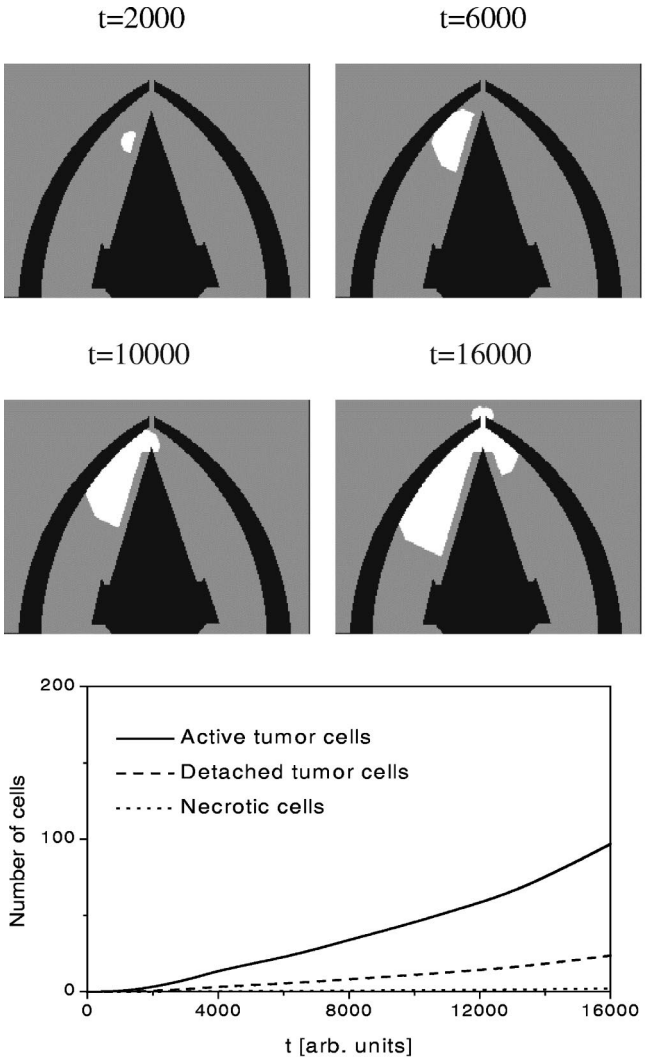

FIG. 4. Same as in Fig. 3 but for $\Gamma = 0.003$. Note the large difference between the scales of the linear plots in Figs. 3 and 4. Likewise the threshold for white (cancerous) areas in the maps has been greatly reduced to enhance the visibility of the cancer-invaded regions.

scale is very different), as evinced by the linear plots. The neoplasm is constrained to grow in the soft tissue since the number of neoplastic cells is never large enough to attack the vocal cord and the cartilage. As a consequence, pressure effects are very strong and growth is very slow (notice the different times in the two figures). The difference in growth speed with respect to the previous case is mostly due to the presence of anatomical constraints since the two cases behave almost identically when no anatomical barriers are present (results not reported for brevity). No increase in volume is observed but, due to the increased mass, the local density increases, in agreement with clinical observations. In the later stages of growth, a horse-shoe shape forms that finally attacks the tissue beyond the tendon. Surgical intervention can usually cure this pathology since the anatomical barriers keep the tumor mass confined for a very long time.

The final mass of the tumor is considerably smaller than in the previous case. The ratio between active, diffusing, and

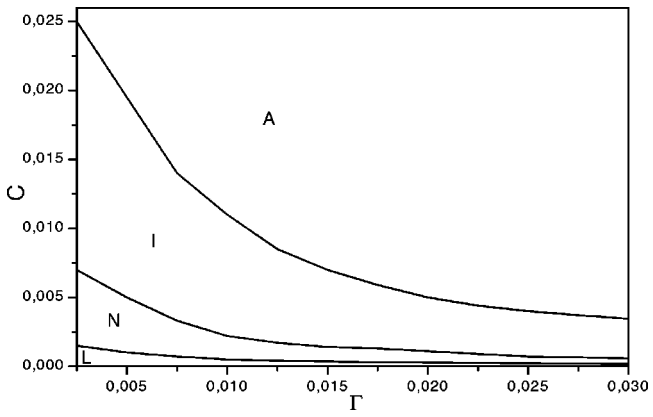

FIG. 5. Phase diagram in the (Γ, C) plane, separating the four regions: latent *L*, noninvasive *N*, invasive *I*, and capable of attacking the cartilage *A*.

necrotic cells is, however, very similar since the thresholds for proliferation and diffusion are the same.

As already remarked, nutrient availability (given by the nutrient concentration C in the blood) is important for the evolution of the tumor [22]. In order to analyze the dependence on both C and Γ, in Fig. 5 we present a ''phase diagram'' of the predicted outcomes. The minimum value for Γ ($\Gamma_{\min} \approx 0.0025$) allows the survival of cells belonging to the initial tumor seed even for a very low availability of nutrients. If C is small, the tumor remains in a state of latency (or dormancy) *L*. For larger values of C the tumor enters first a noninvasive phase *N* and then starts to be invasive *I*. For even larger values of C a transition to a cartilage attacking phase *A* occurs, which shows a strong dependence on Γ. We notice that the latent phase occupies a small area in the phase diagram, which is reasonable, due to the thick network of capillaries distributed inside the connective tissue, which allows adequate nutrient supply even when the density of nutrient in the vessels is low.

B. Neoplasms in the epithelial tissue close to the jaw

As a second application of our approach, we analyze the evolution of a neoplasm originating in the epithelial tissue close to the jaw. The tumor lies on an underlying bone, justifying a $(2+1)$-dimensional analysis.

The jaw is a strong, horse-shoe shaped bone surrounded by soft tissues. Clinical CT scans show dense vascularization. The bone (black in the simulation, first three plots of Fig. 6) appears in the CT scan as a lighter region with an inner dark zone, due to the presence of bone marrow (fourth plot of Fig. 6). Usually CT scans of the jaw show spurious effects such as white spots due to the presence of teeth.

In Fig. 6 we show snapshots at three different times of the growth of a neoplasm in the jaw. We compare the numerical result at $t = 6000$ with a clinical CT scan. The neoplasm, assumed to be very aggressive ($\Gamma = 0.03$) grows mainly in the direction of least resistance, i.e., orthogonal to the bone. However, already at $t \approx 2000$, the tumor starts denting the bone. Nevertheless, the density of neoplastic cells is lower than in the opposite direction (note the lower brightness of the gray scale), since the external part of the bone is avascu-

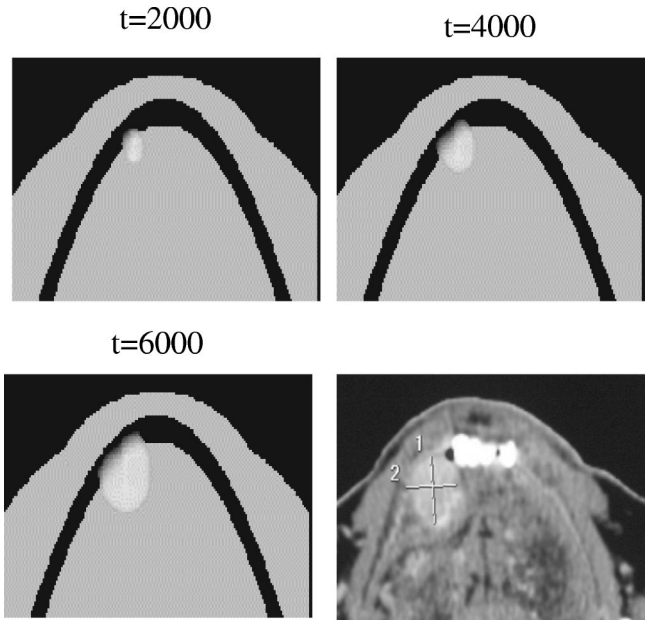

FIG. 6. Snapshots at three different times of the evolution of a neoplasm close to the jaw. Lighter gray tones denote higher density of neoplastic cells. The jaw bone is depicted in black. The bottom row compares the final outcome of the simulation ($t=6000$) to a CT scan (to the right).

lar. Only at later times the tumor reaches the marrow and finds good ground for proliferation.

The agreement with the CT scan is again very encouraging. The elongated final shape of the tumor (marked with a cross in the CT scan) is due to both anatomical constraints and the nutrient gradient. The first factor inhibits proliferation in the upward direction with consequent shape asymmetry. The nutrient gradient, due to the presence of a large vessel (dark spot located approximately in the center of the CT scan), induces the formation of an ellipsoidal (rather than spherical) mass. No necrotic core forms due to the large initial vascularization and reduced tumor infiltration.

IV. CONCLUSIONS

We have presented a physical model, based on the LISA, for the prediction of the spatiotemporal evolution of neoplastic masses in tissues with an irregular distribution of blood vessels and complex anatomical costraints. The approach, suitable for numerical simulations in the framework of parallel processing, treats in a simple way the local mechanisms that affect the tumor behavior.

We mimicked the effect of pressure against the tumoral mass, due to the presence of anatomical constraints, by takine into account the different hardnesses of the various tissues with diffusion coefficients α and $\hat{\alpha}$ for nutrients and tumor cells in different elements of the discretization grid. Maps of $\hat{\alpha}$ describe the tissue consistency, which usually increases when a tumor is present. Aggressive tumors may penetrate regions with large original hardness, affecting its compactness during infiltration. Less malignant neoplasms develop only in soft tissues, do not infiltrate and the neoplastic mass remains bounded by the anatomical barriers (tendons, cartilages, bones, etc.).

In order to validate our model, we simulated the evolution of neoplasms located in the larynx and close to the jaw. In both cases, the numerical results show good qualitative agreement with clinical data (CT scans), showing a good qualitative agreement. Also, by varying only two parameters of the model (nutrient availability and cancer cell affinity) we can predict all the different growth patterns clinically expected. The shape assumed by the neoplasm is generally rather asymmetric, due to both the pressure applied by the rigid tissues and to the formation of gradients in nutrient availability.

A comparison of numerical results with a CT scan at a single time is not sufficient to prove the possibility of making reliable long term predictions with our model. Nevertheless, the capability of our simulations to reproduce complex shapes, as observed for the larynx, implies that our approach includes most major mechanisms that affect tumor morphology and outcomes.

Measurements of the parameters used in the simulations are essential for a quantitative comparison between experimental and numerical results. To this purpose, *in vitro* experiments may be used, e.g., to define the cell proliferation rate [28], which may provide an indirect evaluation of our parameters (e.g., the relationships between the number of transporters and the duplication threshold). *In vivo* measurements can also be performed, e.g., in order to establish the relationship between oxygen tension and proliferation [29] or in the case of tumor cords [30], where the diameter is related to the tumor aggressiveness [31].

ACKNOWLEDGMENTS

We wish to thank Dr. G. P. Pescarmona (Department of Biology, Genetics and Medical Chemistry, Università di Torino, Italy), Dr. M. Motta (Department of Pathological Anatomy and Histology, Ospedale Mauriziano Umberto I, Torino, Italy), and Dr. S. Cirillo (Department of Radiology, Institute of Research and Cancer Care, Candiolo, Torino, Italy) for fruitful discussions. This work was supported by the INFM Parallel Computing Initiative.

[1] C. Suguna, K.K. Chowdhury, and S. Sinha, Phys. Rev. E **60**, 5943 (1999).
[2] G. Fath and Z. Domanski, Phys. Rev. E **60**, 4604 (1999).
[3] *A Survey of Models for Tumor-Immune System Dynamics*, edited by J. A. Adam and N. Bellomo (Birkhäuser, Boston, 1997).
[4] R.M. Shymko and L. Glass, J. Theor. Biol. **63**, 355 (1976).
[5] A.C. Burton, Growth, **30**, 159 (1966).
[6] M. Scalerandi, A. Romano, G.P. Pescarmona, P.P. Delsanto, and C.A. Condat, Phys. Rev. E **59**, 2206 (1999).
[7] S.C. Ferreira, M.L. Martins, and M.J. Vilela, Physica A **272**, 245 (1999).

[8] E. Stott, N.F. Britton, J.A. Glazier, and M. Zajac, Math. Comput. Modell. **30**, 183 (1999).
[9] F. Schweitzer, W. Ebeling, and B. Tilch, Phys. Rev. Lett. **80**, 5044 (1998).
[10] T. Höfer, J.A. Sherratt, and P.K. Maini, Physica D **85**, 425 (1995).
[11] J.C.M. Mombach and J. Glazier, Phys. Rev. Lett. **76**, 3032 (1996).
[12] R.S. Kerbel, Carcinogenesis **21**, 505 (2000).
[13] M.J. Holmes and B.D. Sleeman, J. Theor. Biol. **202**, 95 (2000).
[14] R. Halvorsrud and G. Wagner, Phys. Rev. E **57**, 941 (1998).
[15] A. Brù, J.M. Pastor, I. Fernaud, I. Brù, S. Melle, and C. Berenguer, Phys. Rev. Lett. **81**, 4008 (1998).
[16] H.M. Byrne, J. Math. Biol. **39**, 59 (1999).
[17] A. F. Jones *et al.*, J. Math. Biol. (to be published).
[18] A.J. Perumpanani *et al.*, Physica D **126**, 145 (1999).
[19] P. P. Delsanto, R. Mignogna, M. Scalerandi, and R. Schechter, in *New Perspectives on Problems in Classical and Quantum Physics*, edited by P. P. Delsanto and A. W. Saenz (Gordon and Breach, New Delhi, 1998), Vol. 2, pp. 51–74.
[20] M. Scalerandi, G.P. Pescarmona, P.P. Delsanto, and B. Capogrosso Sansone, Phys. Rev. E **63**, 011901 (2000).
[21] G.P. Pescarmona, M. Scalerandi, P.P. Delsanto, and C.A. Condat, Med. Hypotheses **53**, 497 (1999); M. Magnano *et al.*, J. Surg. Oncol. **74**, 122 (2000).
[22] P.P. Delsanto, A. Romano, M. Scalerandi, and G.P. Pescarmona, Phys. Rev. E **62**, 2547 (2000).
[23] A.J. Perumpanani and H.M. Byrne, Eur. J. Cancer **35**, 1274 (1999); S. Curran and G.I. Murray, *ibid.* **36**, 1621 (2000).
[24] M. Beccaria and G. Curci, Phys. Rev. E **50**, 4560 (1994).
[25] R. Spiro *et al.*, Arch. Otolaryngol. Head Neck Surg. **115**, 316 (1989).
[26] F. Bagatella and L. Bignardi, Acta Oto-Laryngol. **92**, 167 (1981).
[27] E. De Campora and M. Radici, Acta Otorhinolaryngol. Ital. **5**, 491 (1985).
[28] V. Idoyaga Vargas *et al.*, J. Neurol. Sci. **150**, S195 (1997).
[29] M. Nordsmark *et al.*, Int. J. Radiat. Oncol., Biol., Phys. **35**, 701 (1996).
[30] M. Scalerandi, C. A. Condat, and C. Benati (unpublished).
[31] J.V. Moore *et al.*, Eur. J. Cancer Clin. Oncol. **19**, 73 (1984).